Astron. Astrophys. 358, 77–87 (2000)

ASTRONOMY AND ASTROPHYSICS

The Hamburg/ESO survey for bright QSOs

III. A large flux-limited sample of QSOs⋆,⋆⋆

L. Wisotzki, N. Christlieb, N. Bade, V. Beckmann, T. Köhler, C. Vanelle, and D. Reimers

Hamburger Sternwarte, Gojenbergsweg 112, 21029 Hamburg, Germany (lwisotzki@hs.uni-hamburg.de)

Received 3 November 1999 / Accepted 18 February 2000

Abstract. We present a new sample of 415 bright QSOs and Seyfert 1 nuclei drawn from the Hamburg/ESO survey (HES). The sample is spectroscopically 99% complete and well-defined in terms of flux and redshift limits. Optical magnitudes are in the interval $13 \lesssim B_J \lesssim 17.5$, redshifts range within $0 < z < 3.2$. More than 50% of the objects in the sample are new discoveries. We describe the selection techniques and discuss sample completeness and potential selection effects. There is no evidence for redshift-dependent variations of completeness; in particular, low-redshift QSOs – notoriously missed by other optical surveys – are abundant in this sample, since no discrimination against extended sources is imposed. For the same reason, the HES is not biased against QSOs multiply imaged due to gravitational lensing. The sample forms the largest homogeneous set of bright QSOs currently in existence, useful for a variety of statistical studies. We have redetermined the bright part of the optical quasar number-magnitude relation. We confirm that the Palomar-Green survey is significantly incomplete, but that its degree of incompleteness has recently been overestimated.

Key words: galaxies: quasars: general – galaxies: photometry – galaxies: Seyfert – cosmology: observations – surveys

1. Introduction

While the total number of known quasars is growing rapidly, most of these are too faint for detailed investigations. Existing catalogues are mostly inhomogeneous in composition and not representative, featuring disproportionately high fractions of radio-loud, X-ray- and infrared-selected QSOs especially among the brightest known QSOs. To homogeneously sample the bright part of the quasar population in the optical regime, substantial fractions of the extragalactic sky have to be covered with efficient surveying techniques. The only presently available such catalogue, the Palomar-Green Bright Quasar Sample (BQS; Schmidt & Green 1983), is now known to be substantially incomplete (Goldschmidt et al. 1992; Köhler et al. 1997). A similar project in the southern hemisphere, the Edinburgh/Cape Survey (ECS; Stobie et al. 1997), has just produced first output, and the completeness of this survey remains to be assessed. Moreover, both BQS and ECS discriminate against low-z QSOs with extended host galaxies, and the photometric UV excess selection technique confines both surveys to $z < 2.2$ QSOs.

In 1990 we have started the 'Hamburg/ESO survey' (HES), a new wide-angle survey for bright QSOs and Seyferts, as an ESO key programme. The survey is based on digitised objective-prism photographs taken with the ESO Schmidt telescope, covering essentially the entire southern extragalactic sky. QSO candidates are selected with largely automated procedures, minimising human interaction and establishing well-defined input samples for follow-up slit spectroscopy. A description of initial design and first results of the HES was given by Wisotzki et al. (1996; hereafter Paper 1), where also the driving science objectives behind the survey have been listed. A list of 160 newly discovered QSOs and Seyfert 1 galaxies was published by Reimers et al. (1996; hereafter Paper 2). The first flux-limited sample of 55 QSOs, distributed over an effective area of 611 deg^2, was presented and analysed by Köhler et al. (1997), to measure the surface density of bright quasars and to estimate the combined local luminosity function of quasars and Seyfert 1 nuclei.

In this paper we present a major expansion of our earlier work. The survey area has been sixfolded, and the QSO selection techniques have evolved significantly. We have constructed a new flux-limited sample of 415 optically bright QSOs that will be useful for a wide variety of statistical investigations. We describe the selection techniques used to build the sample and discuss its completeness, in comparison with other surveys as well as in terms of expected redshift-dependent selection effects. In providing these details, this paper serves also as a reference for future publications of HES-selected QSO samples. The paper closes with a reassessment of the surface density of bright QSOs. In a companion paper (Wisotzki 2000) we study the impact of this new sample on the bright end of the QSO luminosity function and its evolution. Further work is in progress to follow up on several issues like host galaxy characteristics, radio properties, or the incidence of gravitational lensing events.

Send offprint requests to: L. Wisotzki

⋆ Based on observations made at the European Southern Observatory, La Silla, Chile

⋆⋆ Table A.1 and B.1 are only available in electronic form at the CDS via anonymous ftp to `cdsarc.u-strasbg.fr`

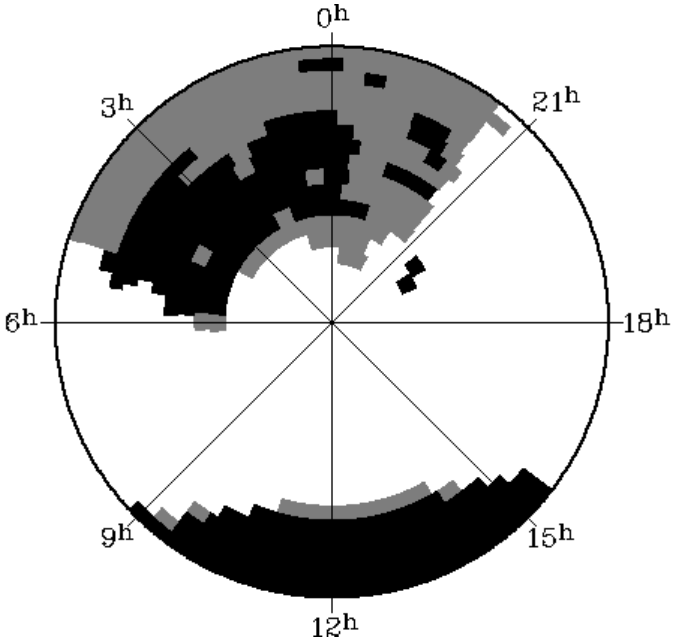

Fig. 1. Distribution of HES survey fields in the southern hemisphere, in area-conserving azimuthal projection. The South pole is in the centre, and meridians of constant right ascension are marked. The black areas correspond to the 207 fields forming the basis for the flux-limited sample, while greyshaded zones indicate further HES fields where survey work is not yet completed. Fields left white are in or too close to the Milky Way.

2. The Hamburg/ESO survey

2.1. Survey area and plate material

Following the installation of the Hamburg/ESO survey, 444 objective prism plates were taken between 1990 and 1998 at the 1 m Schmidt telescope on La Silla. The survey area has been defined chiefly by the need to avoid regions too close to the Milky Way, apart from the initial requirement $\delta < +2\overset{\circ}{.}5$. The basic condition was a column density of Galactic neutral hydrogen in the field centre of $N_H < 10^{21}\,\mathrm{cm}^{-2}$, with the N_H data taken from the collation of Dickey & Lockman (1990), available through the EXSAS software package. Some further fields were excluded because of too high stellar surface densities, as the reduction of effective area due to overlapping spectra increases dramatically with this number. There are 380 ESO fields meeting these criteria, covering a total area of almost $\sim 10\,000\,\mathrm{deg}^2$ in the sky. Fig. 1 shows the distribution of the 380 survey fields in the sky, of which 207 were fully processed at the time of constructing the new sample. This included plate digitisation, reduction, photometric calibration, as well as spectroscopic follow-up observations of quasar candidates to well-defined magnitude limits. These 207 fields are marked in black in Fig. 1.

The photographic material used for the spectral plates was always unfiltered Kodak IIIa-J, giving a spectral range of $\sim$ 3200–5400 Å. The ESO Schmidt objective prism has a reciprocal dispersion of 450 Å/mm at Hγ, allowing for a (seeing-limited) spectral resolution of objective prism spectra as high as 10 Å at Hγ. While in the past such high spectral resolution has always been regarded as not useful for quasar work because of the bright detection limits, it is in fact an extremely well-suited instrumentation to perform an efficient wide-angle search for bright QSOs.

For each spectral plate, a corresponding direct photograph is required. The SERC-J atlas of the southern sky provides a natural counterpart. The atlas has already been fully digitised at the STScI in Baltimore and is readily available as part 1 of 'The Digitized Sky Survey' (DSS)[1] on CD-ROM. Since the nominal centres of spectral and direct plates correspond and the UKST plates are much larger than the ESO plates, there is a 100% match of areas in virtually all fields, even in the (quite common) cases in which the ESO prism plates were found to be decentered by several minutes of arc. The plate scale is nearly the same for ESO Schmidt and UKST. A drawback of the DSS data is that the digitisation grid is rather coarse, allowing for a spatial resolution of $\sim 3''$ at best, much poorer than on the spectral plates. We found that many of the objects appearing extended in the DSS because of two merged stellar images were in fact well separated in the digitised spectral data.

In a survey like this, it is not possible to utilize the entire area of 27 deg^2 formally subtended by the photographic plates for the selection of quasar candidates. Several effects contribute to a reduction of usable area:

- Decentred prism plates leave small gaps between adjacent fields, as the ESO Schmidt plates are too small to always ensure sufficient plate-to-plate overlap.
- Bright stars, large galaxies, and a few globular clusters render certain regions of each plate unprocessable. The same effect occurs if large-scale plate flaws are present.
- Two nearby sources will appear as one single, merged object on the DSS direct image, and the fainter of these will be lost for the input catalogue.
- Most important is the fact that all slitless spectroscopic surveys suffer from losses due to overlapping spectra. These losses are particularly important for the unfiltered high-dispersion spectra of the ESO Schmidt. The loss factor depends strongly on the stellar surface density and thus on Galactic latitude.

We have quantified all these effects, incorporated them into 'effective areas' Ω_{eff}. As a grand average over all fields, the nominal area has to be reduced by roughly 25% to obtain Ω_{eff}; for individual fields the reduction factors range between $< 10\%$ close

[1] Based on photographic data obtained using The UK Schmidt Telescope. The UK Schmidt Telescope was operated by the Royal Observatory Edinburgh, with funding from the UK Science and Engineering Research Council, until 1988 June, and thereafter by the Anglo-Australian Observatory. Original plate material is copyright (c) the Royal Observatory Edinburgh and the Anglo-Australian Observatory. The plates were processed into the present compressed digital form with their permission. The Digitized Sky Survey was produced at the Space Telescope Science Institute under US Government grant NAG W-2166.

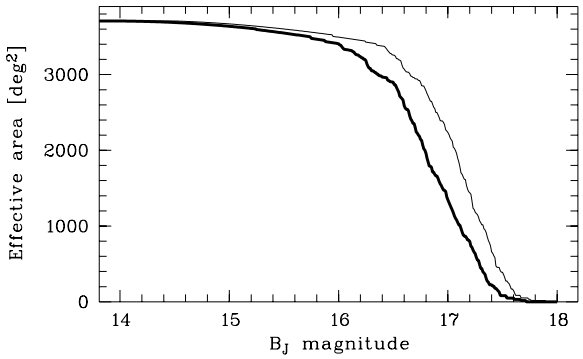

Fig. 2. Effective area of the surveyed region as a function of B_J magnitude (thin line: without correction for Galactic extinction; thick line: with extinction correction).

to the South Galactic Pole and $> 50\%$ in the fields closest to the Milky Way. Because the overlap rate depends on brightness, and because of the field-to-field variations in the magnitude limits, the total effective survey area is a function of apparent magnitude. For the 207 HES plates forming the basis for the sample discussed here, the maximum effective area is 3700 deg^2 for $B_J < 14.5$, decreasing gradually to zero around $B_J \simeq 17.7$ as shown in Fig. 2. A comprehensive listing of the properties of the 207 fields is given in Table A.1 of the appendix.

2.2. Plate digitisation and data reduction

All spectroscopic plates used for the HES were digitised using the Hamburg PDS 1010G microdensitometer, with the hardware upgrades as described by Hagen et al. (1995). However, the two-step digitisation procedure developed for the northern 'Hamburg Quasar Survey', outlined in the same paper, has been replaced for the HES in 1994/95 by full matrix scans of the entire plates. Technical details of the digitisation and reduction procedure will be given elsewhere; here we only comment briefly on a few important properties that are relevant for the discussion below.

Object detection Source catalogues are constructed from the DSS direct images, with a magnitude limit of $B_J \simeq 21$.

Morphological classification Most quasar surveys limit the selection of candidates to objects with 'stellar' morphology. Within the HES, morphological classification into point and extended sources has been installed *only* to optimise the following extraction of spectra.

Wavelength calibration An astrometric transformation between direct and spectral plate establishes for each dataset the precise location of objects and provides wavelength zeropoints with an accuracy of typically $\sim 10\,\mu$m rms, or ± 5 Å near Hγ.

Extraction of spectra We have designed an optimal extraction algorithm of fitting point-spread functions with predetermined widths and positions to the 2–3 central pixels of the submatrix for each object, leaving only the amplitudes as free parameters. This procedure minimises contamination from nearby sources, while at the same time the extraction windows (and subsequent photometry) are limited to apertures of the size of the seeing disk.

Detection limits The formal detection limit is fixed at an internal magnitude corresponding to $2\sigma_b$, where σ_b is the rms background noise in the spectral plate. Typically, this corresponds to a B_J magnitude of ~ 18–18.5. The direct plate input catalogues reach much fainter, so the final candidate search is nearly independent of the object magnitudes on the direct plates.

The bright limit of the survey is set by saturation of the photographic spectra, when UV excess objects are no longer separable. A special extraction scheme for partly saturated spectra allows to extend the bright limit up to $B_J \simeq 11$, yielding a full dynamic range of the HES of $\sim$ seven magnitudes.

3. Selection of quasar candidates

While in most photographic surveys the selection of QSO candidates was limited to one criterion only, the automated processing of multichannel data allows the user to apply several selection criteria in parallel, as first shown by Clowes et al. (1984) and Hewett et al. (1985). For the HES we decided to use an even larger variety of descriptors for the selection, including a certain redundancy with respect to given spectral properties. Two sets of criteria are used, 'colours' and spectral feature detection.

3.1. Colour selection

The first set of criteria mainly exploits continuum properties and can be, to a certain extent, related to traditional photometric colours. The spectral energy distribution is parametrised using the point of flux bisection (i.e. 50% of the flux is located on each side), or 'half power point' (hpp). This concept is applied in three flavours:

`hpp1`: Bisecting point between 3200 and 4840 Å. This number is well correlated with $(U - B)$, cf. below.

`hpp2`: Dito between 3950 and 5400 Å, approximately corresponding to $B - V$.

`hpp3`: Dito between 3520 and 5050 Å. This is a formally redundant feature included to improve the detection rate at faint magnitudes.

`qd` (quartile distance): The distance between the points separating the first and the last 25% of the flux. This feature typically takes large values when the spectrum has composite nature, with a red 'head' and a distinctly 'blue' tail and has been tailored to detect low-z Seyfert galaxies.

This definition of 'colours' has the advantage of being less affected by noise than the simulated broad-band photometry used during the first years of the HES (cf. Paper 1). A similar but much simpler measure was already discussed by Hewett et al. (1995), who employed just a single half-power point bisecting the entire spectra.

The selection of QSO candidates proceeds as follows: For a given dataset (scanned plate), all objects are projected into two-

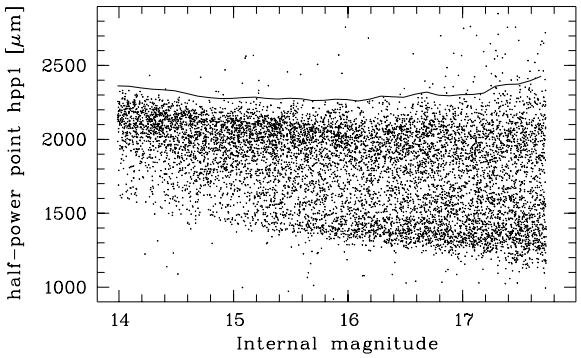

Fig. 3. Selection of UV excess quasar candidates: Distribution of 'colour' hpp1 as a function of internal, uncalibrated magnitude. The solid line separates the UV excess objects from the bulk of normal stars.

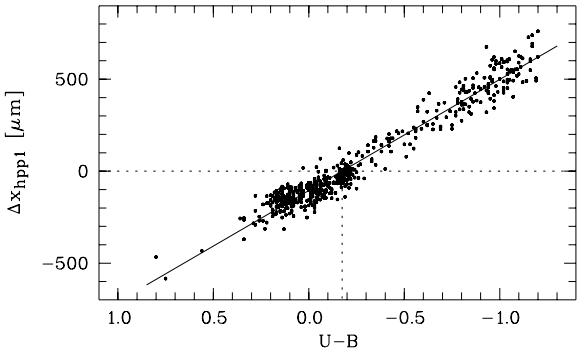

Fig. 4. Comparison of UVX selection criterion with photoelectric photometry: hpp1 distance to selection cutoff vs. photoelectric $(U-B)$. Objects with $\Delta x_{\rm hpp1} > 0$ are selected as UV excess candidates.

dimensional arrays, with the internal PDS magnitude as one, and one of the 'colours' as the other coordinate (cf. Fig. 3). A cutoff-location algorithm then traces the well-defined sharp blue edge of the distribution of Galactic stars, approximately located at spectral types G–F. This yields a polygon adapted to the empirical distribution, independent of systematic variations from plate to plate, and also accounting for magnitude-dependent trends (such as emulsion nonlinearity) within a plate. Objects located on the blue side of the cutoff-tracing curve in each of these feature diagrams are then marked as candidates.

To compare the performance of our colour selection scheme with standard photometric selection, we have used published photolectric *UBV* measurements of OB subdwarfs and metal-poor halo stars found in our fields, taken from the Edinburgh/Cape UV excess survey (Kilkenny et al. 1997) and the HK narrow-band prism survey (Preston et al. 1991). Fig. 4 shows the relative hpp1 colours (distance to actual cutoff) of these stars plotted against $(U-B)$. In this plot, objects above the horizontal dotted line are selected as QSO candidates. The correlation is excellent; it is nearly linear over the entire range, and the rms scatter is only 0.09 mag (a quadratic relation reduces the scatter to 0.08 mag). Notice that the plot was compiled from several photographic plates; hence, the scatter is partly caused by unavoidable plate-to-plate variations, and the true uncertainty of converting hpp1 colours into $(U-B)$ *within* one scan dataset will therefore be even smaller. This astonishingly high accuracy of colour estimation can be explained partly by the fact that, in contrast to traditional photographic photometry, no external calibration is needed; but it also demonstrates the quality and homogeneity of the ESO plate material.

The selection threshold shown in Fig. 4 is equivalent to selecting objects with $(U-B) < -0.18$ (vertical dotted line), considerably less restrictive than the conventional UV excess criterion $(U-B) \lesssim -0.4$ imposed in most photometric surveys. Together with the above uncertainty estimate this implies that of the objects with intrinsic $(U-B) < -0.5$, less than $\sim 1\%$ will be missed by the survey UVX selection criterion.

We note in paranthesis that a similar relation exists between $(B-V)$ and our second continuum 'colour' hpp2. This colour has been included to widen the redshift range sensitive to colour selection schemes (cf. below).

3.2. Feature detection

According to the traditional approach, selecting quasars in sets of slitless spectra means looking for emission-line objects. Although the majority of our objects are selected by colours, we have implemented such a search via a template matching algorithm. This comprises cross-correlation of each continuum subtracted spectrum with Gaussian emission-line templates of various widths, as well as with a differentiating 'break locating' template of zero total flux.

For each line detected by the matching algorithm, a signal-to-noise value is computed as well as line flux and equivalent width; all detections stronger than S/N = 2.5 and with $W_0 > 20\,\mu$m, or ≈ 10 Å at Hγ, are recorded.

A problem with these automatically detected features originates in the high quality of the spectra themselves: At the spectral resolution of the ESO Schmidt objective prism, common late-type stars show already very structured absorption line complexes, in particular in the near UV around and shortwards of the Ca II H+K doublet (which is clearly resolved). The automatically determined pseudo-continuum is systematically too low in such objects, causing many spurious detections of 'emission lines' or 'breaks' that are in fact just caused by absorption complexes. A selection only with respect to the S/N would therefore yield thousands of false detections, and a more refined scheme was required in order to make automated feature detection viable. To accomplish this, all detections in a given scan are represented again as points in two-dimensional feature diagrams, with the template S/N as one and the position in the spectrum as the other coordinate. A cutoff-locating algorithm very similar to that employed in the colour selection provides a separation curve between the tail of the stellar distribution and true outliers. In consequence, the detection threshold is a nontrivial function of wavelength: A typical selection threshold is S/N > 5–6 for most wavelengths, but increases to S/N $\gtrsim$ 15 in narrow wavelength intervals where affected by common stellar absorption features. This makes the effiency of emission-line based quasar selection also depending heavily on redshift z, with certain al-

most 'blind spots' in redshift space. As we discuss below, this becomes relevant only at redshifts $\gtrsim 2.6$, while at all lower z colour techniques are generally more efficient.

3.3. Elimination of false candidates

After applying the primary selection criteria, the number of QSO candidates per plate is typically a few hundred per plate, still considerably higher than the expected number of true quasars. These automatically selected candidates are then subjected to an interactive check at the computer screen, where the extracted spectra are displayed together with the corresponding pixel matrix images of direct and spectral plate. It is generally straightforward to eliminate the dominant contaminations of false, i.e. obviously non-quasar candidates, from these candidate sets.

Plate flaws and artefacts, also satellite trails, ghost images etc. already contribute typically more than 50% of the selected candidates, in fact most of the feature detections. By visual inspection of the direct or spectral plate images, such structures are easily identified.

Blue stars are always the main population in UV excess selected samples. For the magnitudes sampled by the HES, the number ratio between stars and quasars is typically $> 10:1$, further enhanced by the broad range of selection criteria and the relaxed limits. However, the large majority of these stars shows conspicuous Balmer absorption lines easily discernible in the high-resolution spectral data, as illustrated in Fig. 5, and are thus readily removed. For sufficient continuum signal-to-noise ratio even the relatively weak-lined SdB and SdF stars, generally the most notorious contaminating population in quasar surveys, can be identified with high confidence from the objective-prism spectra alone.

3.4. Follow-up spectroscopy

Despite the good spectral resolution of the ESO Schmidt objective prism, slit spectra are generally superior in wavelength coverage, calibration accuracy, and also in signal-to-noise ratio. A spectroscopic follow-up programme for high-grade QSO candidates was started in November 1990 using the 1.52 m, 2.2 m, and 3.6 m telescopes at ESO. The spectra have typically ~ 20 Å resolution and continuum signal-to-noise ratios of $\gtrsim 15$, so that unambiguous classifications and redshifts could be assigned in most cases, without needing to obtain another exposure (for several example spectra see Paper 2). A number of spectra show no evidence of either emission or absorption lines, despite a good S/N. While most of these objects are probably weak-lined white dwarfs, it cannot be excluded that this group contains also a few BL Lac objects. These uncertainties will be probably resolved after a cross-correlation of the HES with the ROSAT All-Sky Survey, which is under way (cf. Bade et al. 1995). At any rate, given the high S/N of most of the spectra it is unlikely that there are unrecognised quasars among these. Objects already listed in the catalogue by Véron-Cetty & Véron (1996 and earlier versions) were not generally observed, except when the catalogue

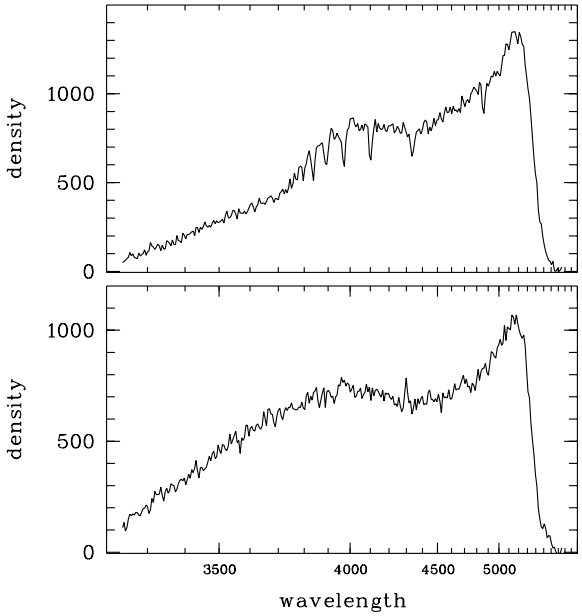

Fig. 5. Example for digitised objective prism spectra, illustrating the potential of using high-dispersion slitless data. The upper spectrum shows a subluminous blue star with narrow Balmer absorption lines, while the lower spectrum represents a low-redshift quasar ($z = 0.15$), devoid of strong emission features except the weak [O II] line at 4300 Å.

entry contained no redshift, or if the objective prism spectrum gave rise to suspicion that the catalogue redshift might be wrong.

As already mentioned in Paper 1, the HES follows a twofold selection strategy: Close to the plate detection limit, only *bona fide* QSO candidates, in particular at high redshift, are followed up spectroscopically. Operational completeness of candidate follow-up is attempted only for a brighter limiting magnitude. This 'completeness limit' corresponds to a minimum S/N of 5 in the spectra, approximately one magnitude brighter than the detection limit. In some fields, the follow-up had to be stopped at a yet brighter but still well-defined limit. Altogether, 587 objects were observed for the flux-limited sample, with only two further sources ($< 0.3\%$) still lacking spectroscopic identification.

An important measure for the efficiency of a quasar survey is the relative number of 'failures' in the follow-up spectroscopy, indicative of the ability to discriminate between quasars and stars. Note that this number as such is not yet an efficiency indicator, as it depends also strongly on the magnitude limit. Brighter surveys inevitably show a higher fraction of stars because of the very different number-magnitude relations of quasars and stars. For example, the Palomar-Green survey for bright ($B \lesssim 16.2$) UV excess objects (Green et al. (1986) contains a stellar fraction of $\sim 93\%$, while three magnitudes fainter the number ratio of UVX stars to quasars is about 1:1 (La Franca et al. 1992). The stellar fraction for the HES colour-selected candidates is $\gtrsim 90\%$ (see above); it is fortunate that most of these objects are SdB stars or DA white dwarfs, since precisely for these classes the recognition of stellar absorption features in the objective prism spectra is extremely efficient. These obviously stellar objects were not even included in the follow-up lists,

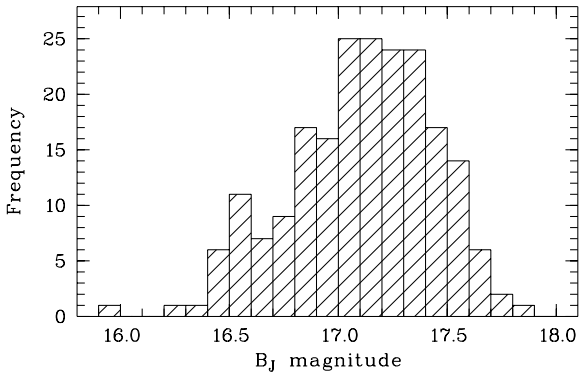

Fig. 6. Distribution of actual B_J magnitude limits for the 207 HES fields used for the complete sample.

leading to a dramatically reduced stellar contamination among the quasar candidates to be observed: Only 189 out of the 587 observed candidates for the 'complete sample' turned out to be stars, most of these of rare or even highly peculiar nature (e.g., magnetic white dwarfs, cf. Reimers et al. 1996). This extremely high success rate of $\sim$ 2:1 is unmatched for an optically bright quasar survey, approaching the efficiencies obtained in X-ray and radio follow-up identification programmes. Note that this rate has been achieved *without* sacrifices in completeness, as it is entirely due to the enhanced ability of the HES to eliminate the stellar contamination.

3.5. Photometry

In contrast to photometric surveys, QSO search on objective prism plates does not *require* prior photometric calibration, as all quantities including colour information can be expressed consistently in internal units. Photometric measurements of all individual sources as well as the determination of survey flux limits, tied to a homogeneous external photometric system, become essential only when statistical quantities such as surface densities and luminosity functions are to be determined. For a wide-angle survey such as the HES, the main difficulty to overcome was the lack of suitable photometric standard stars in most of the survey fields. Although since publication of the HST *Guide Star Photometric Catalogue* (GSPC; Lasker et al. 1990) there are at least a few standard stars known in each ESO field, these stars generally do not cover the magnitude range of interest ($B \lesssim 15$ for the GSPC, while $B = 15$–18 is needed). In an attempt to obtain moderately deep ($B \lesssim 19$) sequences of *all* 380 HES survey fields, we have launched a photometric calibration programme using the ESO/Dutch 90 cm telescope. A full description of the programme will be published elsewhere (Vanelle et al., in preparation). In each field, there are now typically 10–20 calibration stars available within the magnitude range $B = 12$–20, with both B and V photometry available.

With these sequences it was straightforward to compute photometric solutions for the B_J isophotal magnitudes measured in the DSS direct plate scans. However, isophotal magnitudes of extended objects such as low-redshift QSOs with detectable host galaxy fuzz, but also of single point sources with nearby projected neighbouring objects, are systematically too bright. Limiting the photometry to very small apertures was not acceptable because of the small dynamic range and the coarse spatial resolution of the DSS. We therefore decided to seek for less biased photometry of the survey targets.

Our adopted solution was to measure source fluxes in the digitised spectra, by summing up pixel values over the B_J band, and to calibrate these magnitudes against the direct plates data. This approach has several advantages:

- Since the spectral magnitudes are based on the 'PSF amplitude estimator' used for the extraction of spectra, they correspond to a photometric aperture of the size of the seeing disk, thereby maximising the contrast between nucleus and surrounding fuzz in low-z QSOs and Seyferts.
- Flux limits and photometry are defined in the same data sets, minimising incompleteness near the limits due to photometric scatter.
- Quasar selection and photometric measurements correspond to the same epoch, entirely eliminating the effects of variability bias.
- The dynamic range of the spectral plates is much larger than that of the (glass copy-based) DSS data and can be fully exploited not only for selection, but also for photometry.

We estimate the global photometric uncertainty of these measurements to be of the order of 0.2 mag, including all the error sources. This is confirmed by comparing 400 stars with published photoelectric photometry from Kilkenny et al. (1997) and Preston et al. (1991), which gives an overall rms scatter of 0.17 mag. Since this comparison involves over 50 different Schmidt fields, this scatter includes the contribution of zeropoint errors. However, we cannot exclude at present that in a few (< 10) fields with exceptionally poorly sampled photometric sequences the zeropoint uncertainties might be the dominant error sources; we plan to obtain improved sequences for such fields in the future.

Based on this calibration, the definition of flux limits for each survey field is straightforward. The distribution of actual limiting magnitudes for the 207 fields is shown in Fig. 6. The average magnitude limit is $B_J = 17.1$, approximately ~ 1 mag deeper than the PG survey. Variable plate quality and seeing are the two effects chiefly responsible for the spread of flux limits.

To obtain unbiased magnitudes independent of the position in the sky, we have estimated the foreground extinction A_{B_J} from the measured column densities N_H of Galactic neutral hydrogen, using the formula $A_{B_J} = 3.9 \times N_H/58$ where N_H is given in units of $10^{20}\,\mathrm{cm}^{-2}$ (cf. Bohlin et al. 1978). Table A.1 lists N_H and A_{B_J} for each field. The mean extinction value, averaged over all fields, is 0.23 mag.

4. The quasar sample

Altogether, 415 QSOs and Seyfert 1 galaxies were identified in the surveyed area with prism B_J magnitudes brighter than the actual limits given in Table A.1. No luminosity discrimination

between QSOs and Seyferts was applied; all objects displaying broad (FHWM $\gtrsim 1000\,\mathrm{km\,s^{-1}}$) emission lines in their follow-up spectra have been included, as well as all objects classified either as QSO or as Seyfert 1 in the catalogue by Véron-Cetty & Véron (1996). The sample is listed in full in Table B.1 of the Appendix, giving positions, optical magnitudes, and redshifts. A Hubble diagram is shown in Fig. 7, the marginal distribution of redshifts is given in Fig. 9.

This is by far the largest compilation of optically bright quasars existing to date for which well-defined selection criteria and accurate flux limits have been formulated. It increases the earlier HES sample published by Köhler et al. (1997) by a factor of 6 in covered area and by a factor of 8 in sample size, providing a much denser coverage of the Hubble diagram particularly at low redshifts. Note that, although the fields of Köhler et al. (1997) are all located within the present nominal survey area, neither magnitudes nor effective areas are exactly identical. The reasons for this are (i) the change from the B band photometric system to the B_J passband, enforced by the change of direct plate material, and (ii) the recent homogeneous rescanning and re-reduction of all fields. The latter fact caused also a few of the objects of the Köhler et al. sample to be absent in the new sample (mainly because of a slightly different 'overlap' criterion), while some others were added. These changes, however, are minor.

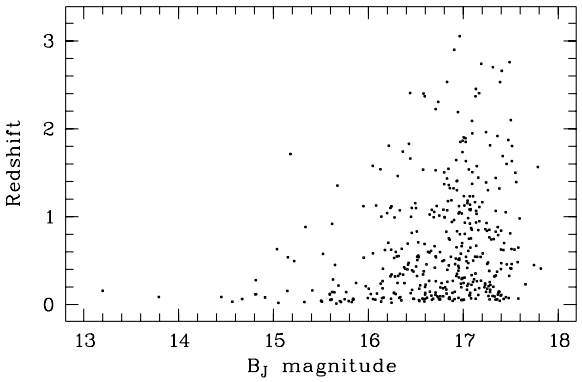

Fig. 7. Hubble diagram of the 415 QSOs and Seyfert 1 galaxies forming the flux-limited sample.

5. Comparison with other surveys

There are not many surveys sensitive to the same domain in the sky and in the magnitude/redshift plane as the HES. While this has allowed the HES to make many 'discoveries', the possibilities to independently test selection efficiency and completeness are necessarily restricted. We shall consider some of the available surveys in turn, and comment briefly on the balance of mutual detections. Apart from the last subsection, we limit this comparison to surveys with well-defined magnitude limits and selection criteria, i.e. we do not consider visually selected samples as these are known to be highly incomplete.

5.1. The Palomar-Green survey

With an average limiting magnitude of $B_{\lim} = 16.16$ and an effective area of more than 10 000 deg^2 (Green et al. 1986), the PG survey is a cornerstone among quasar surveys. Of the ~ 1800 UV excess objects with stellar morphology, 114 detected QSOs and Seyfert 1 galaxies form the 'Bright Quasar Sample' (BQS; Schmidt & Green 1983). There are some 30 PG fields in the region $9^\mathrm{h} < \alpha < 15^\mathrm{h}\,20^\mathrm{m}$, $-12^\circ < \delta < +2\overset{\circ}{.}5$, corresponding to ESO fields 708–725, 780–797 and 850–869. The average PG limiting magnitude in these fields is 16.14 ± 0.18, but with an east-west trend; if bisected at $\alpha = 12^\mathrm{h}$, the limits become $B_{\lim} = 16.31 \pm 0.10$ (east), and $B_{\lim} = 16.03 \pm 0.15$ (west). In these fields, the BQS contains 9 objects that have processable counterparts in the HES (i.e., that are not overlaps etc.), all of which were recovered in the HES candidate selection. However, the HES B_J magnitudes clearly place 5 out of these 9 objects, and possibly another one (depending on the $B - B_J$ correction), *below* the nominal PG limits. On the other hand, the HES has identified 7 further QSOs and Seyferts that were missed in the PG. Two of these are low-z Seyferts which were probably excluded by the morphological selection, yet the other five are clearly luminous QSOs. Only one of them is located close to the magnitude limit, for the others neither the uncertainties in the $B - B_J$ term nor variability can account for this effect. It seems that the PG suffers severely from what appear to be random losses; however, these are partly compensated, with respect to the number counts, by *overcompleteness* from sources below the nominal survey limit.

5.2. The Edinburgh Quasar Survey

The EQS was designed as a multicolour survey over ~ 330 deg^2 close to the equator, covering ESO/SERC fields 789–794 and 861–867 with a limiting magnitude $B < 18.0$ (thus, full overlap of nominal area with the HES). A bright subset of 12 QSOs with $B < 16.5$ was presented by Goldschmidt et al. (1992), based on which they inferred a very high degree of incompleteness for the BQS. The HES quasar sample contains 8 QSOs out of the 12 in the Goldschmidt et al. sample. One entry has to be deleted from this list: for Q 1250−0700 we obtained a slit spectrum which shows an F-type star. The remaining three EQS objects are flagged as overlaps in the HES data. The HES has found one additional QSO brighter than $B = 16.5$ that is not contained in the EQS sample, probably because a prominent host galaxy led to its exclusion as non-stellar. Although the well-known blazar 3C 279 is listed in the HES but not in Goldschmidt et al., this object had in fact been detected by the EQS, but was not considered as proper member of the QSO class (Miller 2000, private communication). A more detailed comparison of EQS and HES including also several unpublished QSOs showed that the photometric scales are in full agreement. On the other hand, the extremely high concentration of bright QSOs found by Goldschmidt et al. (1992) could not be reproduced in the HES, mainly due to the fact that some of the brightest low-z QSOs appear to be systematically brighter in the EQS. The most likely explanation for these differences is that it is caused

by the different photometric techniques used (isophotal in the EQS, point source matching in the HES).

5.3. The 'Large Bright Quasar Survey'

The similarity of the HES selection strategy to that of the LBQS is probably greater than to any other quasar survey (cf. Hewett et al. 1995). Despite its name, the LBQS has mainly yielded intermediate-brightness QSOs, and its bright limit of $B_J > 16.0$ as well as the moderate survey area of $\sim 450\,\mathrm{deg}^2$ allows comparison between HES and the LBQS only over a narrow range of magnitudes around $B_J \simeq 17$. There are 7 fields (ESO field numbers 854, 858, 861, 863, 864, 867, and the SGP field) that both surveys have in common. All 10 LBQS quasars brighter than the HES completeness limit were recovered and are part of the flux-limited sample. The HES has identified further five relatively bright QSOs in these fields that are not part of the LBQS, of which two are at low redshift ($z < 0.1$), and three have apparently been missed by the LBQS. It is of course possible that some of these have been flagged as unprocessable in the LBQS reduction.

5.4. The quasar catalogue of Véron-Cetty & Véron

As a routine task during the HES data reduction, a general comparison with the latest version of the catalogue by Véron-Cetty & Véron (1996) has always been performed. The catalogue was cross-correlated with the input source list from the direct plate object search, followed by a forced extraction of all objects within a large error box of $30'' \times 30''$ around the nominal AGN position – thus avoiding to make any prior assumptions about the integrity of the corresponding spectra. The extracted spectra were inspected, and those contaminated by overlapping neighbour objects were eliminated. Altogether, 143 sources with processable spectra above the 'completeness limits' were identified; of these, 139 had been included into the QSO candidate lists. Of the remaining four, three had actually been selected but were missed in the visual inspection phase, and only one object was missed by the selection criteria. This last object is a bright $z = 3.3$ quasar with a very red and short continuum, but a prominent Lyα line that happens to lie just outside the wavelength region used for the emission line detection, indicating the approximate high-redshift limit for our selection criteria.

6. Redshift-dependent selection efficiency

Optically selected quasar samples are often under suspicion of substantial incompleteness and selection biases varying with redshift, because of the difficulty of discriminating quasar candidates against the outnumbering majority of normal stars. In this section we investigate the importance of such biases for the HES, and discuss the limitations of our adopted QSO survey scheme in this context.

Fig. 8 shows the variation of UV excess with redshift, for the 415 objects in the HES flux-limited sample. This plot has been prepared by converting the excess over the UV selection criterion into a standard ($U - B$) colour, using the empirical relation from Fig. 4. The diagram shows that the mean ($U - B$) varies systematically over the sampled redshift range, but stays always well above the HES selection limit. However, some objects have a very weak UV excess, close to or even below the relatively relaxed selection limit of the HES. These objects entered the sample by matching at least one of the further selection criteria employed by the HES. This is particularly relevant for two groups of objects:

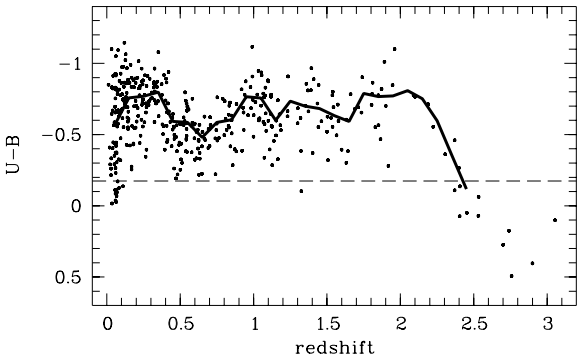

Fig. 8. Distribution of UV excess ($U - B$) as a function of redshift. The thick solid polygon traces the distribution mean in bins of $\Delta z = 0.1$; the horizontal dashed line marks the adopted UVX selection criterion of the HES.

- At low redshifts, Seyfert galaxies tend to lose their UVX as the nuclei get fainter relatively to their host galaxies. To a certain extent, this effect has been counteracted by our dedicated Seyfert criterion 'quartile distance' (cf. Sect. 3.1).
- At the highest redshifts, $z \gtrsim 2.4$, UVX selection of QSOs is known to be impossible. For $z \simeq 2.5$, the redder `hpp2` criterion is still effective; for $z > 2.6$, the objects are selected only by the feature detection algorithm.

Apart from these two extremes, the distribution of measured ($U - B$) values around the mean relation is nearly Gaussian with $\sigma_{U-B} = 0.15$ mag, and the selection boundary is always separated by more than $\sim 2\sigma_{U-B}$. This is qualitatively confirmed by Fig. 8, where at no redshift the distribution appears to be truncated by the selection limit. While the mere presence of some objects with colours close to critical give rise to the suspicion that there may be others that have just been missed, there is no evidence that such objects could make up a sizeable fraction of the population. Note, however, that a more restrictive selection criterion such as $(U - B) < -0.4$ conventionally applied in UVX surveys would have caused severe incompleteness in certain redshift regions.

A further simple and very common test for redshift-dependent selection biases is to look for excess or depletion bins in the observed redshift histogram. The distribution displayed in Fig. 9 shows a steady decline in numbers from low to high redshifts, without indication of significantly high or low bins. The deviations from a smooth 'fit by eye' are entirely consistent with Poissonian ($\sqrt{n}$) shot noise, and there is no evidence for a strong z dependence of the survey selection function.

Notorious for UVX surveys is the regime around $z \approx 0.7$. While the number of HES QSOs in this redshift bin indeed shows a minimum, its value with respect to the neighbouring bins is not significantly low. It cannot be excluded that the selection efficiency for quasars in this redshift region may be somewhat reduced, as the mean colours get slightly redder (Fig. 8). However, similar features of comparable formal significance occur in other redshift bins that do not correspond to identifiable features in the colour distribution and are almost certainly due to statistical fluctuations. This is underlined by the distribution of apparent magnitudes vs. redshifts in Fig. 7, where some of the 'gaps' and 'excesses', including those at $z \approx 0.7$ and $z \approx 1$, occur mainly among the *brighter* objects, while any selection biases would be expected to be stronger close to the limiting magnitude where the S/N is low. Again, this does not necessarily imply a selection function of unity, but it supports our contention that redshift-dependent selection effects are not important for this sample except near the high-z limit.

The situation for $z > 2$ requires a separate discussion. Apart from the colour changes due to a simple shift of the spectrum, real spectra are also affected by intergalactic Lyman forest absorption. Our set of colours is capable, in principle, of selecting QSOs up to redshifts as high as 2.8, but this is too optimistic for real spectra. Nevertheless, *all* quasars with $z < 2.6$ in the current sample are strictly colour-selected, although several have also emission-line detections. In contrast, all $z > 2.6$ objects were detected only by their broad Lyα emission and the corresponding break feature on its blue side. Because of the complicated dependency of the feature detection threshold as a function of wavelength (cf. Sect. 3), the true number of high-z QSOs within the flux limits is necessarily underestimated in the present sample. The degree of this incompleteness depends on redshift, signal-to-noise ratio, but also on the intrinsic properties of the QSOs, the equivalent widths of their Lyα emission lines, and the strength of the Lyman forest break features. Only a detailed simulation study over this multiparameter space will provide reliable estimates of the degree of incompleteness, and generate accurate surface and space densities of quasars with redshifts $\gtrsim 3$.

7. The surface density of bright QSOs

The empirical relation between fluxes and number of sources per unit solid angle is an important diagnostic tool for QSO samples. Once field properties and sample photometry are complete, the cumulative surface density of QSOs brighter than magnitude B_J, $N(< B_J)$, can be easily computed from summing over $1/\Omega_{\rm eff}$ for all relevant sample objects. We have derived the $N(< B_J)$ relation from the 'complete sample' presented above, shown by the solid line in Fig. 10. The abscissa values in this relation are extinction-corrected magnitudes. The bright end of the curve is dominated by the extremely luminous sources 3C 273 and HE 1029−1401, the two brightest QSOs known in the sky, but the main part can be well approximated by a simple power law of slope $\beta = 0.77 \pm 0.01$ ($\log N(< B_J) = \beta B_J + \mathrm{const}$). This slope is slightly steeper

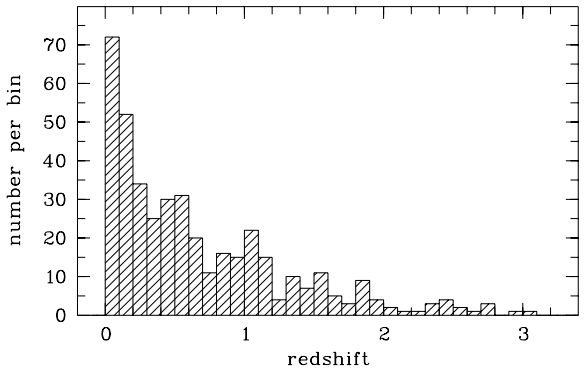

Fig. 9. Redshift distribution of the HES flux-limited sample.

than the extremely flat relation ($\beta = 0.67$) that we had obtained in an earlier analysis (Köhler et al. 1997). The surface densities around $B_J \lesssim 15$ are now somewhat lower, while those for $B_J \lesssim 17$ are even slightly higher than measured before. However, the differences are within the formal uncertainties. The result for the zeropoint is $\log N(< 16) = -1.68$, i.e. we find one QSO brighter than $B_J = 16$ per 48 deg^2.

Comparison relations from other surveys are numerous for fainter magnitudes, but rare for $B_J \lesssim 16.5$. Additional complications arise because various conventions are used for the treatment of low-luminosity and/or low-redshift AGN in the samples: Some authors apply prior cuts in absolute magnitude – e.g., Hartwick & Schade (1990) used only objects with $M_B < -23$ in their compilation. Some others do not count low-redshift AGN, irrespective of absolute magnitude. All these filters are particularly effective at bright apparent magnitudes.

The Palomar-Green BQS (Schmidt & Green 1983) provides the only available optically selected QSO sample with a well-defined flux limit subtending over a similar region in the Hubble diagram. Their published cumulative surface densities include low-redshift and low-luminosity AGN and can be compared to the HES counts of Fig. 10 (the BQS is limited to $z < 2.2$, but this filter has negligible effect at bright magnitudes). However, for a proper comparison the magnitudes of Schmidt & Green need to be corrected for Galactic extinction. We have estimated the mean offset to $\Delta B \simeq 0.2$ from comparing the uncorrected Schmidt & Green counts with the extinction-corrected surface densities listed by Hartwick & Schade (1990), which for $B < 16$ are entirely dominated by the BQS. The BQS magnitudes were shifted by another 0.1 mag in order to approximately correct for the different photometric systems (B_J vs. B; cf. Hewett et al. 1995), so that the resulting number-magnitude relation for the BQS, shown by the small circles in Fig. 10, is based on an adopted magnitude scale $B_J \simeq B_{\rm BQS} - 0.3$.

The surface densities of the BQS are below those of the HES at all covered magnitudes, whereas the inferred slopes are virtually identical. Therefore the ratio of surface densities is nearly constant, $N_{\rm HES}/N_{\rm BQS} = 1.48 \pm 0.06$. While this excess is highly significant in itself, it is much lower than the earlier claimed incompleteness rate of a factor 3 or more by Goldschmidt et al. (1992) or by ourselves (Köhler et al. 1997). As

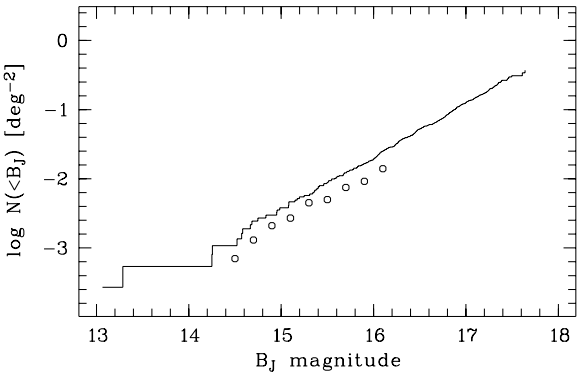

Fig. 10. Cumulative surface density $N(< B_J)$ of bright QSOs as a function of magnitude, without cut in redshift or luminosity. The small circles show the corresponding relation from Schmidt & Green (1983), with magnitudes corrected as discussed in the text.

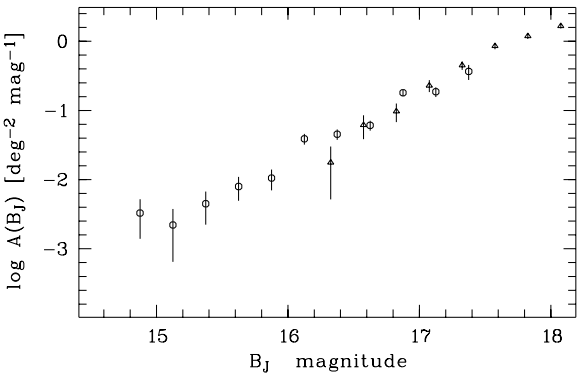

Fig. 11. Differential surface densities of QSOs for the redshift interval $0.2 < z < 2.2$, with error bars from Poisson statistics. Circles denote the HES measurements, triangles show the corresponding data from the LBQS (Hewett et al. 1995).

discussed above, the small EQS sample used by Goldschmidt et al. (1992) is basically a subset of the new HES sample, and their high number seems to constitute a statistical fluctuation. Neither Goldschmidt et al. nor Köhler et al. included Galactic extinction corrections. For the Köhler et al. sample, this would have reduced the inferred incompleteness to a factor $\sim 2.4 \pm 0.5$, statistically consistent with the new value of 1.5 on the 2σ level. It is possible that incompleteness in the BQS is higher for low-luminosity sources, but the direct object-to-object comparison in the overlapping area does not suggest a strong effect. For the present paper we wish to limit this discussion to an overall comparison without splitting samples according to nuclear luminosities, which is problematic without going into the details of comparing our point-source with the BQS isophotal magnitudes. This way we also avoid the complications of a model-dependent conversion to absolute magnitudes. We are currently investigating the host galaxy properties of HES and BQS selected QSOs, which will allow us to understand the possible selection effects in much greater detail.

These new results show with high statistical significance that the BQS is incomplete, but also that the degree of incompleteness has recently been overestimated (a similar conclusion was reached by Mickaelian et al. 1999). On the other hand, our cross-comparison between HES and BQS in overlapping fields has yielded a significant contamination of the BQS with objects fainter than the nominal limits. It thus appears that there is also evidence for *overcompleteness* in the BQS, to a much higher degree than the 15% estimated by Schmidt & Green (1983). The HES–BQS comparison suggests that up to $\sim 50\%$ of the BQS quasars may be affected; in that case, the *true incompleteness* of the BQS would be again at least by a factor of $\gtrsim 2$. To assess the origin of this overcompleteness is difficult. One possibility was suggested by Köhler et al. (1997) in order to explain the different luminosity function slopes, invoking subtle photometric biases favouring moderately extended low-redshift QSOs over real point sources. Alternatively or additionally, the photometric errors in the PG survey might simply be much larger than assumed by Schmidt & Green (1983).

At fainter magnitudes, the HES counts are in excellent agreement with most other surveys. As an example, in Fig. 11 we compare the HES *differential* number counts for the redshift range $0.2 < z < 2.2$ to the same relation for the LBQS published by Hewett et al. (1995). Since the LBQS magnitudes are also given in the B_J system, no photometric transformation is required; a small shift of the LBQS values, by ~ 0.1 mag towards brighter magnitudes, has been applied to correct for Galactic extinction neglected by Hewett et al. The derived surface densities are statistically consistent in all magnitude bins. The brightest LBQS value seems to be somewhat low, possibly indicating incompleteness caused by saturation effects during plate digitisation with the APM machine as discussed by Hewett et al., but even that data point is not formally inconsistent with the HES.

8. Conclusions

The Hamburg/ESO survey is an ongoing project that provides substantial improvements over previous searches for optically bright QSOs. We have constructed a new flux-limited quasar sample useful for a wide variety of statistical studies, consisting of 415 objects distributed over 3700 deg^2 in the sky. Greatest care was taken to minimise selection biases that could lead to redshift-dependent incompleteness. Key properties of the HES in this respect are (i) very relaxed UV excess selection criteria, equivalent to $(U - B) < -0.18$, (ii) the small errors of determining the UV excess in individual objects, and (iii) the high spectral resolution of the ESO objective prism spectra which ensures low stellar contamination without sacrifices in completeness.

Comparing the sample with the results of other surveys, in terms of general number counts as well as by detailed comparison of common survey regions, we find no evidence that the HES might miss a sizeable fraction of the known QSO population, within its redshift limits. The surface density of detected bright quasars, for given magnitudes, is consistent with most recently published work, but the HES sample greatly improves the statistics at very bright magnitudes. We confirm that the Palomar-Green BQS is incomplete (although the degree of incompleteness has been overestimated in the past), but alert the

reader that there is also evidence for significant overcompleteness.

Several precautions were taken to reduce potential selection biases associated with low-redshift QSOs. Unlike most other optical QSO surveys, there is no discrimination of objects with extended morphological structure; these objects are subjected to the same selection criteria as the point sources. In the extraction of spectra, nuclear properties are enhanced relative to possibly 'red' galaxy contributions. This also affects the derived magnitudes which are dominated by the nuclear emission. Furthermore, a specific selection criterion has been implemented that is sensitive to 'Seyfert-like' spectral shapes. All these factors enable the HES to produce the first well-defined optically selected samples of low-z QSOs and bright Seyfert 1 nuclei. At the same time, selection biases against gravitationally lensed QSOs are avoided.

The HES substantially improves the sampling in the high-luminosity, high-redshift domain unaccessible to traditional UV excess surveys. While the number of $z > 2.5$ sources in the present flux-limited sample is still small, there is a large reservoir of unambiguously detected high-z quasars. By using dedicated flux limits optimised for these objects, combined with a detailed determination of the survey selection function, the total number of bright QSOs in the redshift range $2.5 \lesssim z \lesssim 3.3$ that are part of a well-defined flux-limited sample will be increased by at least an order of magnitude in the near future.

Acknowledgements. Thanks to Drs. T. Beers and D. Kilkenny who made the results of their photoelectric photometry available in digital form, and to Dr. L. Miller for allowing us to compare results with unpublished data from the Edinburgh Quasar Survey. We are indebted to Dr. H.-J. Hagen who developed and maintained the operating software to perform the full-matrix digitisation of Schmidt plates with the Hamburg PDS. The Hamburg/ESO survey would not have been possible without the continued support by ESO staff members, in particular H.-E. Schuster, B. Reipurth, and O. and G. Pizarro who took all the Schmidt plates. Substantial observing time was allotted to this project as ESO key programme 02-009-45K. Parts of this work were supported by the DFG under grants Re 353/33 and Re 353/40. We also acknowledge support from BMBF/DLR grants 05-5HH41A and 50 OR 9606 O.

Appendix A: HES survey fields

Table A.1 lists all 207 Hamburg/ESO survey fields used in this investigation. The first two columns list the field number in the standard ESO/SERC numbering system, and the ESO plate number of the objective prism plate. Next given are right ascension and declination of the nominal field centres, in B1950 coordinates. Note that the actual plate centres may deviate from these nominal positions by several arc minutes. The following column gives the limiting magnitudes per field ('completeness limit' = 5σ detections) as obtained from the photometric calibration. The last two entries feature the column density of neutral hydrogen in $10^{20}\ \mathrm{cm}^{-2}$ and the adopted correction for Galactic extinction in the B_J band.

Appendix B: the QSO sample

Table B.1 presents the flux-limited sample of 415 QSOs and bright Seyfert 1 galaxies selected from the Hamburg/ESO survey. The designation is listed in the first two columns: first the standard HE + B1950 coordinate string used by the HES, followed by the name as it appears in the catalogue of Véron-Cetty & Véron (1996). The next columns give J2000 equatorial coordinates obtained from the DSS plate solutions, and the ESO field number where the QSO was found. The following two columns list the redshifts and a flag indicating if the redshift was derived from our own slit spectroscopy; otherwise, the z value from Véron-Cetty & Véron (1996) was used. The final two columns contain the small-aperture B_J apparent magnitudes, and extinction-corrected B_J values.

References

Bade N., Fink H.H., Engels D., et al., 1995, A&AS 110, 469
Bohlin R.C., Savage B.D., Drake J.F., 1978, ApJ 224, 132
Clowes R.G., Cooke J.A., Beard S.M., 1984, MNRAS 207, 99
Dickey J.M., Lockman F.J., 1990, ARA&A 28, 215
Goldschmidt P., Miller L., La Franca F., Cristiani S., 1992, MNRAS 256, 65p
Green R.F., Schmidt M., Liebert J., 1986, ApJS 61, 305
Hagen H.J., Groote D., Engels D., Reimers D., 1995, A&AS 111, 195
Hartwick F.D.A., Schade D., 1990, ARA&A 28, 437
Hewett P.C., Irwin M.J., Bunclark P., et al., 1985, MNRAS 213, 971
Hewett P.C., Foltz C.B., Chaffee F.H., 1995, AJ 109, 1498
Kilkenny D., O'Donoghue D., Koen C., Stobie R., Chen A., 1997, MNRAS 287, 867
Köhler T., Groote D., Reimers D., Wisotzki L., 1997, A&A 325, 502
La Franca F., Cristiani S., Barbieri C., 1992, AJ 103, 1062
Lasker B.M., Sturch C.R., McLean D.J., Jenkner H., 1990, AJ 99, 2019
Mickaelian A.M., Goncales A.C., Véron-Cetty M.-P., (1999), Véron P., Astrophysics 42, 1
Preston G.W., Shectman S.A., Beers T.C., 1991, ApJS 76, 1001
Reimers D., Köhler T., Wisotzki L., 1996, A&AS 115, 235 (Paper 2)
Reimers D., Jordan S., Beckmann V., Christlieb N., Wisotzki L., 1998, A&A 337, L13
Reimers D., Jordan S., Koester D., et al., 1996, A&A 311, 572
Schmidt M., Green R.F., 1983, ApJ 269, 352
Stobie R.S., Kilkenny D., O'Donoghue D., et al., 1997, MNRAS 287, 848
Véron-Cetty M.-P., Véron P., 1996b, ESO Sci.Rep. 17, 1
Wisotzki L., 2000, A&A, in press
Wisotzki L., Köhler T., Groote D., Reimers D., 1996, A&AS 115, 227 (Paper 1)